# The addition of boron to melt-spun Fe-6.5%Si ribbons

Gaoyuan Ouyang<sup>1,\*</sup>, Roger Claude<sup>2</sup>, Alexander Kovar<sup>2</sup>, Ben Hillard<sup>1</sup>, Matthew J. Kramer<sup>1,2</sup>, Iver E. Anderson<sup>1,2</sup>, and Jun Cui<sup>1,2</sup>

<sup>1</sup>Ames National Laboratory, US Department of Energy, Ames, Iowa, 50011, USA <sup>2</sup>Department of Material Science & Engineering, Iowa State University, Ames, Iowa, 50011, USA \*Authors for correspondence. gaoyuan@iastate.edu

#### **Abstract**

Fe-6.5%Si has higher electrical resistivity, lower magnetocrystalline anisotropy, and lower magnetostriction than traditional Fe-3.2%Si silicon steel. The reduced iron losses of Fe-6.5%Si render it a highly favorable candidate for high-speed motors and transformers. However, large-scale production of wide Fe-6.5%Si tape by rapid solidification can be challenging mainly due to its high melting point. In this work, boron is alloyed to Fe-6.5%Si to reduce its melting temperature and interfacial energy to improve the alloy's processability. Boron additions from 0.01 wt% to 2.24 wt% into Fe-6.5%Si and its effect on ribbon thickness, grain size, magnetic, and mechanical properties were studied. Minor boron alloying significantly changed the melt pool stability and wetting on the quench wheel and in turn increased the quench rate with minimum impact on the magnetic saturation and ductility. Boron addition of less than 0.06 wt% was also found beneficial to the magnetic property of the alloy by lowering both its hysteresis and eddy current losses.

Keywords — Microstructure; Rapid solidification; Soft magnetic materials; Saturation magnetization.

#### Introduction

The soft magnetic market for motors, transformers, and power electronics is dominated mainly by electrical steel (Fe-3.2%Si, wt.%), with a market of \$26.28B in 2022 and a compound annual growth rate of 5.95%. Fe-3.2%Si gained popularity mainly due to its excellent performance/cost ratio and processability. With the increasing demand for higher power densities, newer generation electric machines are designed to operate at higher frequencies. Such highfrequency operation can only be effective if the iron losses of the materials can be controlled, which depends heavily on the thickness, electrical resistivity, and domain structure of the soft magnetic material. Though Fe-3.2%Si has a favorable saturation magnetization as high as 2.0 T, its electrical resistivity is only 52  $\mu\Omega$  cm<sup>2</sup>, which can limit its efficiency at high frequencies. Though the thickness, grain structure, and domain structure can all play a role in the iron loss for soft magnetic materials, one of the most important factors is the electrical resistivity of the material itself. The electrical resistivity of iron can be significantly increased by alloying with metalloid elements. By far, the most potent element in increasing the electrical resistivity of iron discovered so far is silicon<sup>3</sup>. With increased Si content, the electrical resistivity of Fe-6.5%Si increases by almost double, contributing to much lower iron losses at high frequencies without compromising the raw material cost 4. However, the increased Si content promotes the preferred pairing of the silicon and iron atoms resulting in B2 and D0<sub>3</sub> ordering from the disordered A2 crystal structure<sup>4</sup>. Fe-6.5%Si is too brittle to be processed if it is allowed to be ordered under normal processing conditions typical of Fe-3.2%Si. Research has shown that Fe-6.5%Si can be made ductile if the ordering can be bypassed by rapid cooling<sup>5,6</sup>. Rapid solidification is suitable for ductile Fe-6.5%Si ribbon production, but there is a limitation on the width and surface quality of the ribbon. This challenge mainly originated from the high melting point of Fe-6.5%Si, which is ~400 °C higher than a typical amorphous alloy that can be mass-produced by planar flow casting. The ribbon quality is also affected by the melt pool behavior on the quench wheel related to factors such as high surface tension and liquid viscosity<sup>7</sup>.

Boron is known to form multiple eutectics in the Fe-Si-B system according to their ternary phase diagram, which helps reduce the melting point. Though how boron affects the surface tension of iron silicon melt was not reported, it was known to reduce the surface tension of iron alloys at 1550°C8. Similar behavior (surface tension reduction) is expected

for iron silicon melt with boron alloying, which can lead to better wetting according to Young's equation<sup>9</sup>. Boron is also expected to reduce the viscosity of the melt, as it is known that boron oxide reduces the viscosity of mixed oxide<sup>10</sup>. Reducing surface tension and viscosity by boron alloying suggest better flow characteristics leading to better processability. Boron alloying to Fe-6.5%Si is not new. Kim et al. <sup>11</sup> pioneered by adding minor amounts (75 ppm to 530 ppm) of boron to rolled Fe-6.5%Si plates. They point out that boron alloying helps increase the grain boundary cohesion and grain refinement, which enables the warm rolling (~500 °C) of Fe-6.5%Si sheets<sup>11,12</sup>. Fu et al.<sup>13</sup> studied the boron alloying into directional solidified Fe-6.5%Si. They showed that boron helps increase the alloy's undercooling, homogenization, strength, and ductility. However, a better understanding of the boron alloying in the processability, magnetic, and mechanical properties, especially in melt-spun Fe-6.5%Si ribbons, is lacking. The present study aims to investigate the effect of boron alloying on the processing and physical properties of Fe-6.5%Si alloys fabricated by arc melting and melt spinning.

### Materials and methods

Fe-6.5%Si was first pre-alloyed by arc melting of high-purity iron and silicon chunks (>99.9%) in an arc furnace under an argon atmosphere. Then boron was alloyed into the pre-alloyed Fe-6.5%Si by melting it with high-purity boron chunks. The boron chunks were covered by Fe-6.5%Si to minimize the mass loss (<0.1% mass loss after melting). The boron added to the sample ranged from 0.01 to 2.24 wt%. The samples were flipped at least three times to ensure homogeneity during each arc melting. The arc melted buttons were then drop cast into 10 mm diameter rods. The melt spinning was done using a custom-built melt spinner. The charge was melted to 1650 °C inside a quartz crucible using induction heating before being injected onto a rotating copper wheel spinning at 20m/s with an overhead pressure of 120 Torr. The nozzle orifice was 0.81 mm in diameter, and the melt spinning chamber was filled with 1/3 of He after 3 vacuum flushes. To probe the melt spinning process, a 12-bit complementary metal-oxide semiconductor (CMOS) high-speed camera was set up and focused on the side profile of the ribbon as it was being produced.

The melting behavior of the alloys was measured by differential scanning calorimetry (NETZSCH, DSC 404). The heating rate was 10 °C/min. The cross-sectional micrographs of the samples were taken using a scanning electron microscope (SEM) (Teneo, FEI Inc) equipped with an energy-dispersive X-ray spectroscopy (EDS) detector. The X-ray diffraction (XRD) patterns were collected via Bruker DaVinci D8 system equipped with a Cu target. The microhardness tests were conducted on polished cross-sections using a microhardness tester (LECO LM 247AT). The magnetic properties of the alloys were measured using Vibrating Sample Magnetometer (VSM) (Versalab, Quantum Design, Inc.) up to 3 Tesla magnetic field. The closed-loop magnetic measurement was done using a computer-automated soft magnetic test station (model SMT-700, KJS Associates/Magnetic Instrumentation) with a single-strip test fixture. The melt-spun ribbons were annealed in a sealed quartz tube filled with Ar at 1100 °C for 2 hours and then were assembled into a plate 18 mm wide by 65 mm long for the magnetic measurement. A MgO coating was applied to the ribbons to prevent inter-ribbon adhesion during annealing and was removed after the annealing. The densities of the alloys needed for the flux density calculation were measured on drop-casted samples using Archimedes' method.

#### **Results and discussion**

The DSC curves in Fig. 1a show the melting behavior of the alloys. The melting onset of the liquidus is depressed, accompanied by the formation of a eutectic phase with boron alloying. The eutectic temperature (1145~1160 °C) in Fig. 1a correlates well with the eutectic temperature in Fe-B or Fe-Si-B phase diagram. The onsets of the liquidus and the eutectic are plotted in Fig. 1b as a function of boron content. The liquidus onset for the Fe-6.5%Si was 1415 °C, and it was lowered by 15 °C with 0.21 wt% of boron, which was further lowered to 1350 °C with 1.10 wt% of boron. When boron is added to 2.24 wt% (close to the eutectic composition), the melting point of Fe-6.5%Si is fully depressed to the eutectic temperature of 1145 °C, which is 270 °C lower than its original melting point. The 2.24 wt% (10 at%) of boron addition will bring the alloy into the amorphous region, as reported by Luborsky et al<sup>14</sup>. The formation of an amorphous structure is confirmed on melt-spun ribbon with 2.24 wt% boron alloying through XRD studies (not shown). By estimating the heat of fusion or change in enthalpy in melting (area under the curve), Fig. 1c shows the relative fractions of the solid solution and eutectic phases. The amount of eutectic phase increases rapidly with increasing

boron additions. The amount of eutectic is ~14.2% with 0.21 wt% of boron addition, where it increases to 54.1% and 100% with 1.10 wt% and 2.24 wt% of boron additions, respectively.

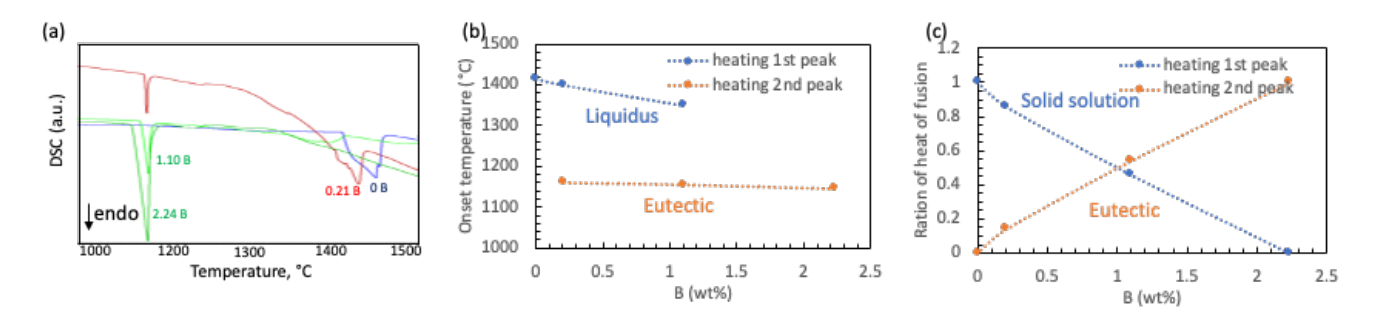


Fig. 1. Melting characteristics of the Fe-6.5%Si alloy with various levels of boron additions. (a) DSC curves showing the melting points of the alloys where the amount of boron additions are labeled by the curves; (b) the melting onset of the liquidus phase and the intermetallic phase as a function of boron content; (c) the ratio of heat of fusion between the solid solution phase and the eutectic phase.

The Fe-rich side of the Fe-B phase diagram consists of Fe<sub>2</sub>B and (Fe) solid solution with a maximum solubility of 0.02 at% with a eutectic temperature of 1175°C <sup>15</sup>. According to the 10 at.% Si vertical section of Fe-Si-B pseudo-binary phase diagram, a ternary eutectic is present between (Fe), Fe<sub>2</sub>B, and Fe<sub>2.7</sub>Si<sub>0.3</sub>B. The eutectic temperature is 1112 °C. The eutectic temperature is in good agreement with the lower temperature peak by the DSC (~1150 °C), considering a higher Si% (12.14 at%) in Fe-6.5%Si alloy. The formation of intermetallics and its eutectics (especially in Fig. 2d) in the as-cast samples can be identified in the XRD patterns and the SEM microstructure in Fig. 2. The shift in the XRD for the 0.02 wt%B is reversed compared to rest suggests that the composition of the matrix is not taking up all the solutes. The micrographs show that the fraction of intermetallic phase increases with increasing boron addition. The XRD patterns and the phase diagram analysis suggest that the intermetallic could be Fe<sub>2.7</sub>Si<sub>0.3</sub>B <sup>16</sup>. The intermetallic effectively pins the gain growth of the Fe-6.5%Si solid solution phase, which may lead to lower eddy current losses at high frequencies. The cooling rate (~10<sup>6</sup> °C/s) for the as-spun sample seems fast enough to prevent intermetallic precipitation where only BCC solid solution phase is present in the XRD patterns (XRD pattern not shown).

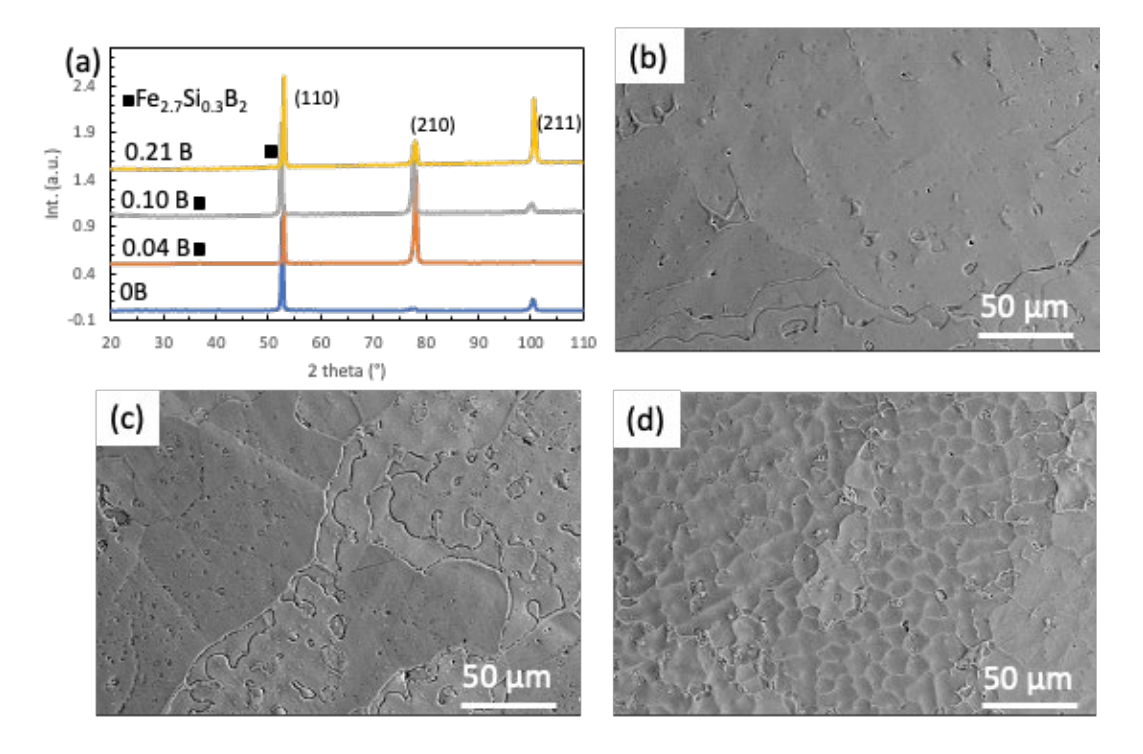


Fig. 2. Phase and microstructure of the Fe-6.5%Si alloys with various levels of boron additions. (a) XRD patterns of the patterns with the amount of boron added labeled; SEM images of the samples with (b) 0.04 wt%, (c) 0.10 wt%, and (d) 0.21 wt% of boron additions.

To study the physical properties of the alloy with boron alloying, the saturation magnetization Ms and the microhardness were measured. As shown in Fig. 3, overall, the Ms drops almost linearly with boron alloying. Boron, being a paramagnetic element, dilutes the ferromagnetic moment of iron. The drop in Ms is minor, being only 0.05 T/at% B. The rise in Ms with 0.04 wt% boron alloying is interesting. Such an increase in magnetization with a small amount of boron was also reported by Wan and Chen<sup>17</sup> in their boron-added non-oriented electrical steel. Below a critical concentration, boron segregation in the grain boundary was believed to result in increased grain coarsen, leading to higher flux density (permeability) and lower core losses<sup>17</sup>. The microhardness of the samples does not follow a monotonic relationship with boron content. Rather, the hardness drops initially, then rise with increasing boron content. It is well known that hardness is closely related to grain size (Hall–Petch relationship) and intermetallic formation. The formation of the intermetallic phase and refined grains (Fig. 2) with boron alloying (> 0.10 wt%) are responsible for the increase in hardness observed. The hardness of Fe-6.5%Si is also closely related to its ordering degree <sup>18</sup>. A lower ordering degree resulting from faster cooling can significantly reduce the hardness of Fe-6.5%Si <sup>19</sup>. Boron alloying forms a low melting eutectic that aids the cooling of Fe-6.5%Si. The lower ordering degree due to faster cooling is responsible for the initial (B ≤ 0.10 wt%) hardness reduction. Such an initial drop in hardness is consistent with the reported increased ductility with minor amounts of boron additions <sup>11,13</sup>.

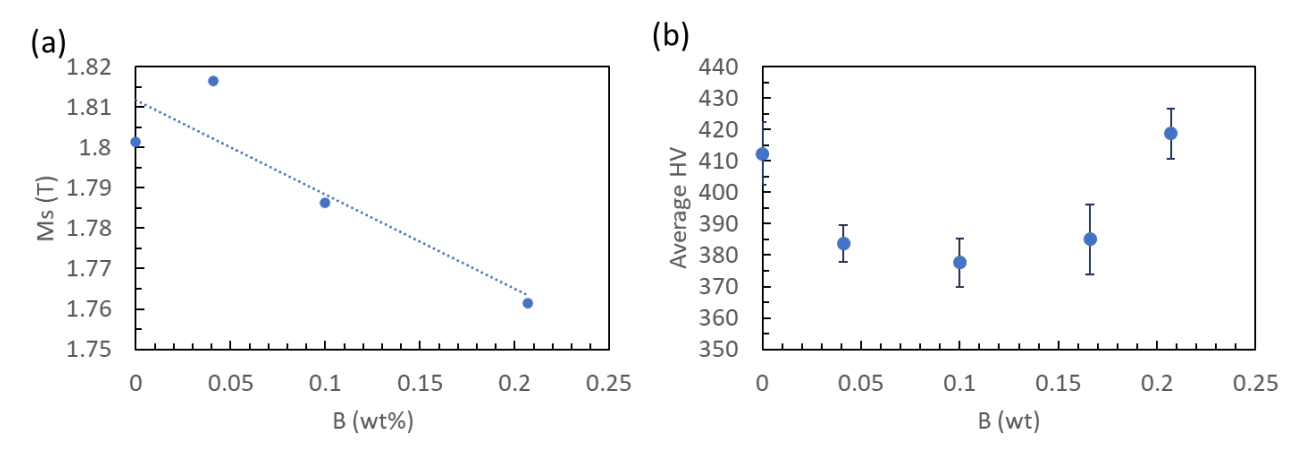
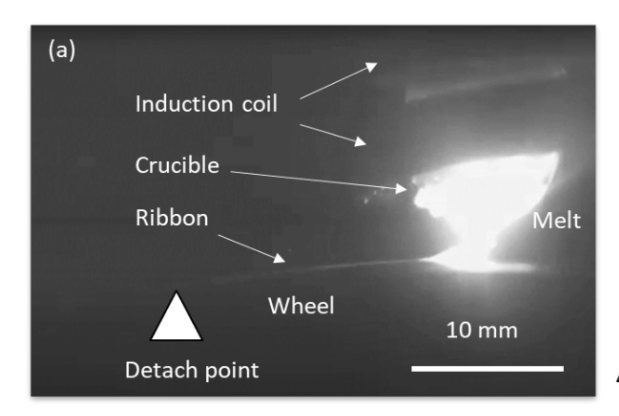


Fig. 3. Saturation (a) and hardness (b) of the drop cast Fe-6.5%Si alloys with varying levels of boron additions.

High-quality ribbon/tape production (i.e., uniform thickness and width) of Fe-6.5%Si depends heavily on the flow characteristics of the alloy during the melt spinning or planar flow casting process. An essential parameter for the flow characteristics is the melt-wheel contact distance. For Fe-6.5%Si, a longer wheel contact distance resulted from a more stable melt pool is desirable as it improves the cooling of the ribbon. Longer wheel contact distance also has significant practical importance. It helps heat management during manufacturing (by avoiding red hot ribbons) and aids in controlling detached angles when a ribbon detachment mechanism is used. The ribbon(melt)-wheel contact distance was evaluated via a high-speed camera by imaging the side profile of the ribbon as it is being formed. The triangle symbol in Fig. 4 marks where the ribbon is detached from the wheel. It quantitatively shows an improved wheel contact with boron alloying. This is direct evidence of better flow characteristics from added boron owing to improved wetting and reduced viscosity. Boron alloyed ribbons also are longer and more continuous, with improved surface quality.



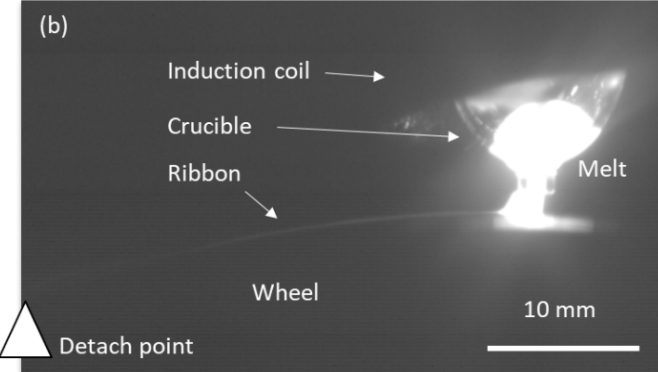


Fig. 4. High-speed camera snapshot of the melt spinning process of Fe-6.5%Si with (a) no boron and (b) 0.21 wt% of boron addition. The melt, the ribbon, the detach point, and various parts of the melt spinner are labeled.

A parallel plate bending test was also performed to characterize the ductility of the as-spun ribbon. This test quantifies the bending strain of the sample when bending the ribbon between two plates until the ribbon breaks. The distance of the two parallel plates is noted, and together with the thickness of the ribbon were used to calculate the bending strain. Due to the high ductility of the ribbon, we count the number of ribbons that break when the two plates completely close, i.e., the spacing of the parallel plates becomes zero. The likelihood of fracture (out of 10 tests for each composition) are 0%, 10%, 10%, and 50% for the 0%, 0.046%, 0.1%, and 0.207% boron alloyed samples, respectively. It suggests that minor boron alloying ( $\leq$  0.10 wt%) has a minimum impact on the ductility of the samples. However, there is a noticeable ductility decrease when 0.21 wt% boron is added due to excess intermetallic formation.

Table 1. The likelihood of fracture during the parallel plate test when the two plates completed touch each other for the Fe-6.5%Si alloy ribbons with various levels of boron additions.

Ribbon's boron content (wt%)	Likelihood of fracture (%)
0	0
0.05	10
0.10	10
0.21	50

The as-spun Fe-6.5%Si ribbons are known to have high hysteresis losses due to their refined grain size<sup>4</sup>. Therefore, the melt-spun ribbons were fully annealed for a more representative magnetic property and iron loss measurement. Fig. 5 shows that the permeability of the alloy under direct current (DC) condition increases to a maximum at 0.01 wt% boron addition, then it drops with higher levels of boron additions. The coercivity of the alloy was also the lowest at 0.01wt% boron addition, and then it increased when more boron was added. For the alternating current (AC) 400HZ condition, the iron loss decreased significantly initially (31.7% coreless reduction in the case of 0.01 wt% boron addition) then it started to increase. For the range (up to 0.06 wt%) of boron addition shown in Fig. 5, the boron addition significantly lowers the DC hysteresis losses by increasing permeability and lower coercivity. Ribbon thickness measurement (Fig. 5b) also reveals that the boron-added samples are thinner, which leads to lower classical eddy current loss. Therefore, the minor boron-added Fe-6.5%Si annealed ribbons showed a lower total iron loss, which is a sum of hysteresis loss, classical eddy current loss, and anomalous loss. The reduction of ribbon thickness with boron addition directly resulted from the improved wetting and lower viscosity of the melt, as described above. Typically, the hysteresis loss tends to be higher on thinner ribbons because of the more refined boundary condition for grain growth when annealed. Here, it is apparent that the boron additions in Fe-6.5%Si facilitated the grain growth during

the annealing though the ribbon thickness is thinner. The enhanced boron-facilitated coarsening behavior during annealing is in good agreement with the work of Wan and Chen<sup>17</sup> where they also observed larger grain size and higher flux densities in their boron-added non-oriented silicon steels. There has been a dilemma for iron loss minimization for melt-spun ribbons: if the ribbon is thin, it may have higher hysteresis loss due to limited grain growth; if the ribbon is thick, it may have high eddy current loss. Boron addition offers a solution to the dilemma, which is the key to lower iron losses.

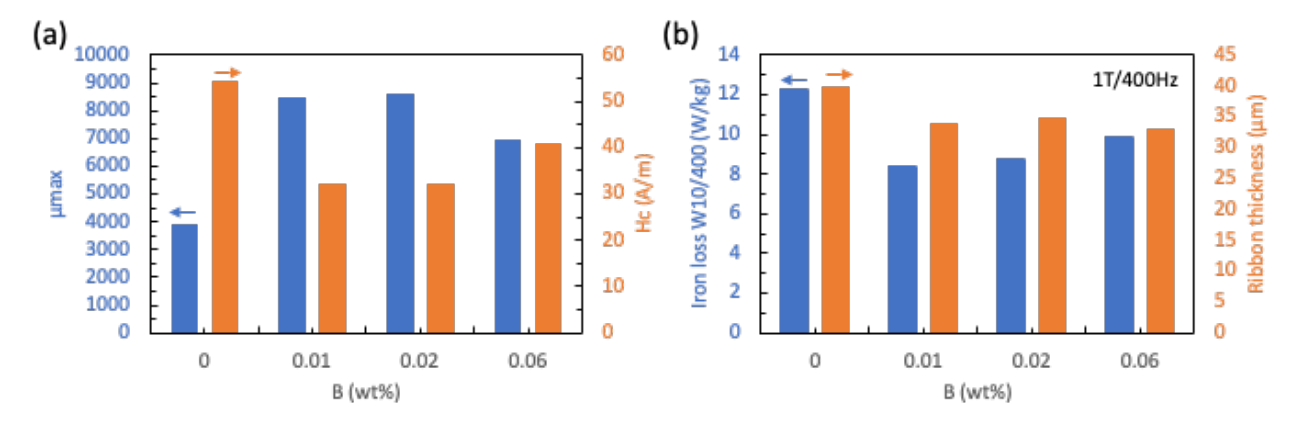


Fig. 5. Soft magnetic properties of the annealed Fe-6.5%Si ribbons with varying levels of boron additions. (a) maximum permeability ( $\mu$ ) and coercivity (H<sub>c</sub>) of samples under a maximum magnetic flux density of 1 Tesla in DC; (b) iron losses of the samples at 1T magnetic flux density and AC 400Hz and the thickness of the samples.

## **Summary**

This paper investigated the effect of boron addition on the processing, magnetic, and mechanical properties of Fe-6.5%Si. It is found that the boron addition resulted in eutectic formation, which is beneficial for the viscosity reduction of the Fe-6.5%Si alloy. Boron addition improves the processability of the alloy resulting in improved melt/ribbon-wheel contact with enhanced cooling. The resulting ribbon is more continuous and longer, with improved surface quality. A critical amount of boron addition to the Fe-6.5%Si was found to be around 0.06 wt%. Below this critical amount, improved DC and AC magnetic properties were observed, which can relate to the boron-segregated grain boundary that facilitated grain growth and improved wetting. The hardness of the alloy with less than 0.06 wt% of boron is also lower, owing to the improved solidification characteristics. Above 0.06 wt%, or in some cases, 0.10 wt% of boron addition, the formation of intermetallic negatively impacts the alloy's physical properties, resulting in lower saturation, higher hardness, and decreased ductility. Overall, minor boron addition was found to be an effective processing additive to Fe-6.5%Si production by melt spinning, which can improve the quality of the ribbon/tape. It is also a valid addition to improve the magnetic properties of the alloy with both lowered hysteresis and eddy current losses.

## Acknowledgment

This work was supported by the U.S. Department of Energy, Office of U.S. Department of Energy's Vehicle Technologies Office. The research was performed at the Ames Laboratory, which is operated for the U.S. DOE by Iowa State University under contract # DE-AC02-07CH11358.

## **Conflict of interest statement**

On behalf of all authors, the corresponding author states that there is no conflict of interest.

#### References

- Electrical Steel Global Market Report 2022. https://www.reportlinker.com/p06282671/Electrical-Steel-Global-Market-Report.html?utm\_source=GNW.
- 2. Bozorth, R. M. Ferromagnetism. Ferromagnetism (1993).
- 3. Tumanski, S. *Handbook of magnetic measurements*. (CRC press, 2016).
- 4. Ouyang, G., Chen, X., Liang, Y., Macziewski, C. & Cui, J. Review of Fe-6.5 wt%Si high silicon steel—A promising soft magnetic material for sub-kHz application. *J. Magn. Magn. Mater.* **481**, 234–250 (2019).
- 5. Arai, K. & Tsuya, N. Ribbon-form silicon-iron alloy containing around 6.5 percent silicon. *IEEE Trans. Magn.* **16**, 126–129 (1980).
- Liang, Y. F. et al. Fabrication of Fe-6.5wt%Si Ribbons by Melt Spinning Method on Large Scale. Adv. Mater. Sci. Eng. 2015, e296197 (2015).
- 7. Kramer, M. J. *et al.* Rapid solidification and metallic glass formation Experimental and theoretical limits. *J. Non-Cryst. Solids* **353**, 3633–3639 (2007).
- 8. Korobeinikov, I., Chebykin, D., Seetharaman, S. & Volkova, O. Effect of Boron Micro-alloying on the Surface Tension of Liquid Iron and Steel Alloys. *Int. J. Thermophys.* **41**, 56 (2020).
- 9. Makkonen, L. Young's equation revisited. J. Phys. Condens. Matter 28, 135001 (2016).
- 10. Cai, Z., Song, B., Li, L., Liu, Z. & Cui, X. Effects of B2O3 on Viscosity, Structure, and Crystallization of Mold Fluxes for Casting Rare Earth Alloyed Steels. *Metals* **8**, 737 (2018).
- 11. Kim, K. N. et al. The effect of boron content on the processing for Fe–6.5wt% Si electrical steel sheets. *J. Magn. Magn. Mater.* **277**, 331–336 (2004).
- 12. Ye, F., Liang, Y. F., Wang, Y. L., Lin, J. P. & Chen, G. L. Fe-6.5wt.%Si High Silicon Steel Sheets Produced by Cold Rolling. *Mater. Sci. Forum* **638–642**, 1428–1433 (2010).
- 13. Fu, H., Zhang, Z., Wu, X. & Xie, J. Effects of boron on microstructure and mechanical properties of Fe-6.5 wt.%Si alloy fabricated by directional solidification. *Intermetallics* **35**, 67–72 (2013).
- 14. Luborsky, F., Becker, J., Walter, J. & Liebermann, H. Formation and magnetic properties of Fe-B-Si amorphous alloys. *IEEE Trans. Magn.* **15**, 1146–1149 (1979).

- 15. Hallemans, B., Wollants, P. & Roos, J. R. Thermodynamic Reassessment and Calculation of the Fe-B Phase Diagram. *Int. J. Mater. Res.* **85**, 676–682 (1994).
- 16. Chaban, N. F. & Kuz'ma, Y. B. Phase equilibria in the systems manganese-silicon-boron and iron-silicon-boron.

  Inorg MaterTransl Neorg Mater 6, 883–884 (1970).
- 17. Wan, Y. & Chen, W. Effect of boron content on the microstructure and magnetic properties of non-oriented electrical steels. *J. Wuhan Univ. Technol.-Mater Sci Ed* **30**, 574–579 (2015).
- 18. Ouyang, G. *et al.* Effects of Solidification Cooling Rates on Microstructures and Physical Properties of Fe-6.5%Si Alloys. *Acta Mater.* **205**, 116575 (2021).
- 19. Ouyang, G. *et al.* Effect of wheel speed on magnetic and mechanical properties of melt spun Fe-6.5 wt.% Si high silicon steel. *AIP Adv.* **8**, 056111 (2018).